IAHR AIRH

Journal of Hydraulic Research Vol. 46, No. 1 (2008), pp. 35–44

Similitude and scale effects of air entrainment in hydraulic jumps

Similitude et effets d'échelle de l'entraînement d'air dans les ressauts hydrauliques

HUBERT CHANSON, IAHR Member, Professor, *Department of Civil Engineering, The University of Queensland, Brisbane, QLD 4072, Australia. Fax: (61 7) 33 65 45 99; e-mail: h.chanson@uq.edu.au; Url: http://www.uq.edu.au/~e2hchans/ (author for correspondence)*

CARLO GUALTIERI, Assistant Professor, *Hydraulic and Environmental Engineering Department, University of Napoli, Via Claudio 21, 80125 Napoli, Italy*

ABSTRACT
A hydraulic jump is characterized by some strong turbulence and air entrainment in the roller. New measurements were performed in two channels in which similar experiments with identical inflow Froude numbers and relative channel widths were conducted with a geometric scaling ratio of 2:1. Void fraction distributions showed the presence of an advection/diffusion shear layer in which the data followed an analytical solution of the diffusion equation for air bubbles. The data indicated some scale effects in the small channel in terms of void fraction and bubble count rate. Void fraction distributions implied comparatively greater detrainment at low Reynolds numbers yielding to lesser overall aeration of the jump roller. Dimensionless bubble count rates were significantly lower in the smaller channel especially in the mixing layer. The study is believed to be the first systematic investigation of scale effects affecting air entrainment in hydraulic jumps using an accurate air–water measurement technique.

RÉSUMÉ
Un ressaut hydraulique est caractérisé par une turbulence et un entraînement d'air importants dans le rouleau. De nouvelles mesures ont été effectuées avec deux canaux dans lesquels on a entrepris des expériences similaires avec des nombres de Froude identiques à l'amont et des largeurs relatives de canal dans un rapport géométrique de 2:1. Les distributions de fractions de vide ont montré la présence d'une couche de cisaillement d'advection/diffusion dans laquelle les données suivaient une solution analytique de l'équation de diffusion pour des bulles d'air. Les données ont indiqué quelques effets d'échelle dans le petit canal en termes de fraction de vide et de taux de décompte de bulles. Les distributions de fraction de vide impliquaient comparativement un débarquement plus grand aux faibles nombres de Reynolds, indiquant une moindre aération globale du rouleau de ressaut. Les taux sans dimension de décompte de bulles étaient sensiblement inférieurs dans le plus petit canal particulièrement dans la couche de mélange. On pense que cette étude constitue la première recherche systématique sur les effets d'échelle affectant l'entraînement d'air dans les ressauts hydrauliques, en utilisant une technique précise de mesure air-eau.

Keywords: Hydraulic jumps, air entrainment, physical modelling, similitude, scale effects.

1 Introduction

In an open channel, the transition from super- to sub-critical flow is a flow singularity, called hydraulic jump, that is characterised by a sharp rise in free-surface elevation, strong turbulence and air entrainment in the roller (Figs 1 and 2). Although the hydraulic jump has been investigated experimentally for nearly two centuries, little information is available on the air–water flow properties in the jump flow. Historically air entrainment in hydraulic jump was investigated in terms of the air demand (Kalinske and Robertson, 1943; Wisner, 1965). Contributions on the air–water flow properties included Rajaratnam (1962), Resch and Leutheusser (1972), Chanson (1995), Mossa and Tolve (1998), Chanson and Brattberg (2000), and Murzyn *et al.* (2005). These studies however did not investigate specifically possible scale effects affecting the air entrainment and advection processes.

This study presents new experimental results to compare these with existing data and to present new compelling conclusions regarding air entrainment and air–water flow properties in hydraulic jumps. Similar experiments were repeated in two flumes with identical inflow Froude numbers and relative channel widths, and the results provide new informations on scale effects affecting void fraction and bubble count rate distributions. The study is focused in the developing flow region (i.e. $(x - x_1)/d_1 < 25$) of hydraulic jumps with partially-developed inflow conditions.

2 Dimensional analysis and similitude

Analytical and numerical studies of the air–water flow properties in hydraulic jumps are difficult considering the large number

Revision received January 2, 2007/Open for discussion until August 31, 2008.

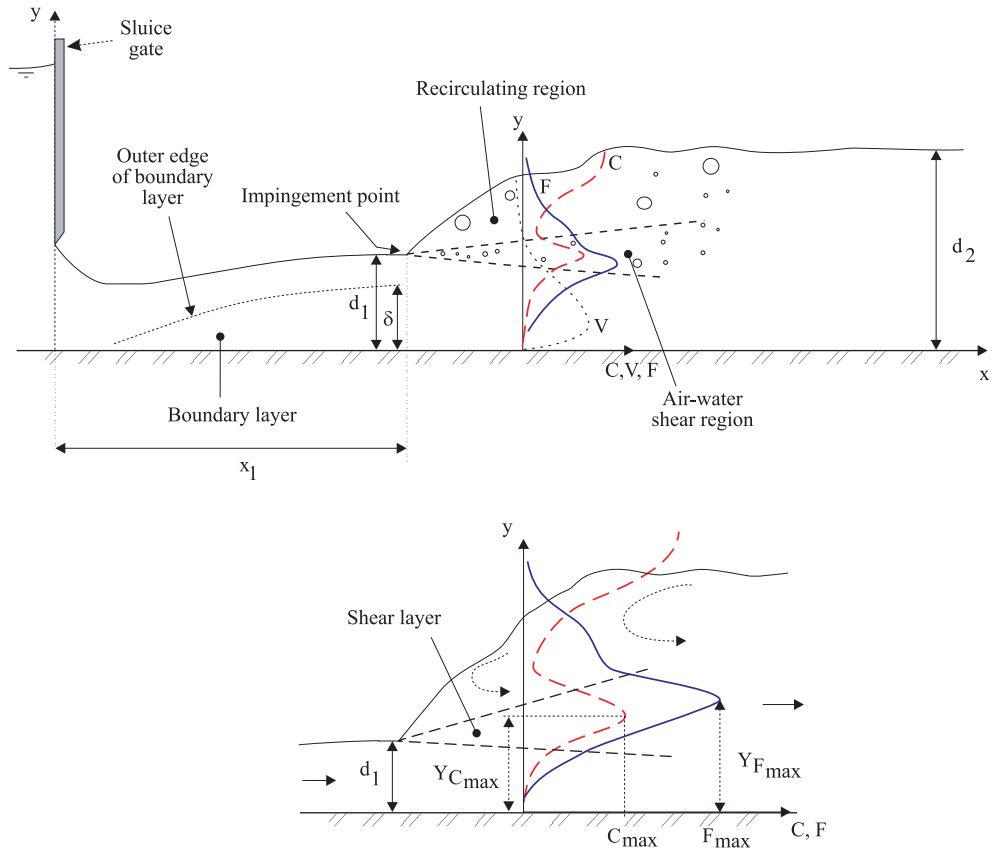

Figure 1 Definition sketch of hydraulic jump with partially-developed inflow conditions.

(A) (B)

Figure 2 High-speed photographs of hydraulic jump ($Fr_1 = 6.5$) (A) Hydraulic jump in the small flume (inflow conditions: $Fr_1 = 6.5$, $Re_1 = 2.7\text{E}+4$, $V_1 = 2.2$ m/s, $d_1 = 0.012$ m, $W = 0.25$ m) flow from left to right (shutter speed: 1/500 s). (B) Hydraulic jump in the large flume (inflow conditions: $Fr_1 = 6.5$, $Re_1 = 7.1\text{E}+4$, $V_1 = 3.1$ m/s, $d_1 = 0.023$ m, $W = 0.5$ m) flow from left to right (shutter speed: 1/500 s).

of relevant equations. Experimental investigations of air–water flows are often performed with geometrically similar models, but model studies must be designed based upon a sound similitude. For a hydraulic jump in a horizontal, rectangular channel, a simplified dimensional analysis points out that the parameters affecting the air–water flow properties at a position (x, y, z) are:

(a) the fluid properties such as the air and water densities ρ_{air} and ρ_w, the air and water dynamic viscosities μ_{air} and μ_w, the surface tension σ and the gravity acceleration g,
(b) the channel properties including the width W,
(c) the inflow properties such as the inflow depth d_1, the inflow velocity V_1, the characteristic turbulent velocity u'_1, and the boundary layer thickness δ.

Therefore the air–water flow properties may be expressed as:

$$C, F, V, u', \ldots = F_2(x, y, z, d_1, V_1, u'_1, x_1, \delta, W, g, \rho_{air}, \rho_w, \mu_{air}, \mu_w, \sigma, \ldots) \quad (1)$$

where C is the void fraction, F is the bubble count rate, V is the velocity, u' is a characteristic turbulent velocity, x is the coordinate in the flow direction measured from the nozzle, y is the vertical coordinate, z is the transverse coordinate measured from the channel centreline, and x_1 is the distance from the upstream gate (Fig. 1). In addition, biochemical properties of the water solution may be considered. If the local void fraction C is known, the density and viscosity of the air–water mixture may be expressed in terms of the water properties and void fraction, hence the parameters ρ_{air} and μ_{air} may be ignored.

Since the relevant characteristic length scale is the upstream flow depth d_1, Eq. (1) may be transformed in dimensionless terms:

$$C, \frac{F * d_1}{V_1}, \frac{V}{\sqrt{g * d_1}}, \frac{u'}{V_1}, \cdots = F_2\left(\frac{x - x_1}{d_1}; \frac{y}{d_1}; \frac{z}{d_1}; \frac{x_1}{d_1}; \frac{V_1}{\sqrt{g * d_1}}; \frac{\rho_w * V_1^2 * d_1}{\sigma}; \rho_w * \frac{V_1 * d_1}{\mu_w}; \frac{u'^1}{V_1}; \frac{\delta}{d_1}; \frac{W}{d_1}; \cdots\right) \quad (2a)$$

In Eq. (2a), the dimensionless air–water flow properties (left handside terms) at a dimensionless position $(x/d_1, y/d_1, z/d_1)$ are expressed as functions of the dimensionless inflow properties and channel geometry. In the right handside of Eq. (2a), the fifth, sixth, and seventh terms are the inflow Froude, Weber and Reynolds numbers, respectively. Any combination of these numbers is also dimensionless and may be used to replace one of the combinations. In particular one parameter can be replaced by the Morton number $M_o = g * \mu_w^4/(\rho_w * \sigma^3)$. The Morton number is a function only of fluid properties and gravity constant, and it becomes an invariant if the same fluids (air and water) are used in both model and prototype:

$$C, \frac{F * d_1}{V_1}, \frac{V}{\sqrt{g * d_1}}, \frac{u'}{V_1}, \cdots = F_3\left(\frac{x - x_1}{d_1}; \frac{y}{d_1}; \frac{z}{d_1}; \frac{x_1}{d_1}; \frac{V_1}{\sqrt{g * d_1}}; \rho_w * \frac{V_1 * d_1}{\mu_w}; \frac{u'^1}{V_1}; \frac{\delta}{d_1}; \frac{W}{d_1}; \frac{g * \mu_w^4}{\rho_w * \sigma^3}; \cdots\right) \quad (2b)$$

2.1 Dynamic similarity and scale effects

In a geometrically similar model, true dynamic similarity is achieved if and only if each dimensionless parameters has the same value in both model and prototype. Scale effects may exist when one or more dimensionless terms have different values between model and prototype.

In the study of free-surface flows including the hydraulic jump, a Froude similitude is commonly used (e.g. Henderson, 1966; Chanson, 2004). That is, the model and prototype Froude numbers must be equal. But the entrapment of air bubbles and the mechanisms of air bubble breakup and coalescence are dominated by surface tension effects, while turbulent processes in the shear region are dominated by viscous forces. Dynamic similarity of air entrainment in hydraulic jumps becomes impossible because of too many relevant parameters (Froude, Reynolds, and Morton number) in Eq. (2). But no systematic study was yet conducted to assess the extent of scale effects affecting air entrainment in hydraulic jump flows.

It is worth commenting that the above analysis does not account for the characteristics of the instrumentation. The size of the probe sensor, the scanning rate and possibly other probe characteristics do affect the minimum bubble size detectable by the measurement system. Up to date, all systematic studies of scale effects affecting air entrainment processes were conducted with the same instrumentation and sensor size in all experiments. The probe sensor size was not scaled down in the small size models. The present study is no exception and it is acknowledged that this aspect might become a limitation.

3 Experimental channels and instrumentation

New experiments were performed in the Gordon McKay Hydraulics Laboratory at the University of Queensland (Table 1). The first channel was horizontal, 3.2 m long and 0.25 m wide. Both bottom and sidewalls were made of 3.2-m-long glass panels. This channel was previously used by Chanson (1995) and Chanson and Brattberg (2000). The second channel was horizontal, 3.2-m-long and 0.5 m wide. The sidewalls were made of 3.2-m-long glass panels and the bed was made of 12-mm-thick PVC sheet. Both channels were fed by a constant head tank.

Table 1 Summary of experimental flow conditions

Channel (1)	d_1 (m) (2)	x_1 (m) (3)	V_1 (m/s) (4)	W (m) (5)	Fr_1 (6)	Re_1 (7)	Comments (8)
Small flume							Glass bottom and sidewalls
	0.0133	0.5	1.86	0.25	5.1	2.5 E + 4	Run 051115
	0.012		2.2		6.5	2.7 E + 4	Run 060202
	0.0129		3.0		8.4	3.8 E + 4	Run 051122
Large flume							Glass sidewalls and PVC bed
	0.0265	1.0	2.6	0.50	5.1	6.8 E + 4	Run 051202
	0.0231		3.1		6.5	7.1 E + 4	Run 060127
	0.0238		4.14		8.6	9.8 E + 4	Run 051206

Notes: $Fr_1 = V_1/\sqrt{g * d_1}$; $Re_1 = \rho_w * V_1 * d_1/\mu_w$; x_1: distance between the upstream gate and jump toe.

Further details on the experiments were reported in Chanson (2006).

3.1 Instrumentation

In the narrow flume, the flow rate was measured with a 90° V-notch weir which was calibrated on-site with a volume-per-time technique. In the 0.5-m-wide channel, the water discharge was measured with a Venturi meter which was calibrated *in situ* with a large V-notch weir. The percentage of error was expected to be less than 2%. The water depths were measured using rail mounted pointer gauges with an accuracy of 0.2 mm.

The air–water flow properties were measured with a single-tip conductivity probe (needle probe design). The probe consisted of a sharpened rod (platinum wire $\varnothing = 0.35$ mm) which was insulated except for its tip and set into a metal supporting tube. It was excited by an electronic system (Ref. AS25240) designed with a response time less than 10 μs and calibrated with a square wave generator. The probe vertical position was controlled by a fine adjustment system with an accuracy of 0.1 mm.

A sensitivity analysis was performed to assess the effects of sampling duration T_{scan} and sampling rate F_{scan} on the hydraulic jump air–water properties, namely the void fraction and bubble count rate. The sensitivity tests were conducted with sampling times within $0.7\,s \leq T_{scan} \leq 300\,s$ and a sampling frequency between $600\,s \leq F_{scan} \leq 80{,}000$ Hz. The results showed that the sampling frequency had little effect on the void fraction for a given sampling duration, but the bubble count rate was drastically underestimated for sampling rates below 5–8 kHz. Furthermore the sampling duration had little effect on both void fraction and bubble count rate for scan periods longer than 30 s to 40 s. In the present study, the probe was scanned at 20 kHz for 45 s at each sampling location.

Additional informations were obtained with digital cameras Panasonic™ Lumix DMC-FZ20GN (shutter: 8–1/2000 s) and Olympus™ Camedia C700 (shutter: 4–1/1000 s), and a digital video-camera Sony™ DV-CCD DCR-TRV900 (speed 25 fr/s, shutter: 1/4–1/10,000 s).

3.2 Experimental procedure and inflow conditions

Preliminary clear-water velocity measurements were performed in both flumes using a Prandtl-Pitot tube ($\varnothing = 3.3$ mm). The results showed that the supercritical inflow in both flumes was partially–developed for all investigated flow conditions (Table 1). The relative boundary layer thickness δ/d_1 was about 0.5–0.6 depending on the inflow conditions.

The two channels were designed to be geometrically similar based upon a Froude similitude with undistorted scale. The geometric scaling ratio was $L_r = 2.0$ between the narrow and wide channels, where L_r is the ratio of prototype to model dimensions. Similar experiments were conducted for identical Froude numbers $Fr_1 = V_1/\sqrt{g * d_1}$, relative channel width W/d_1 and relative gate-to-jump toe distance x_1/d_1. Measurements were performed at identical cross-sections $(x - x_1)/d_1$ in both channels with several inflow Froude numbers (Table 1). The present study was focused in the developing air–water flow region: i.e., $(x - x_1)/d_1 \leq 25$.

4 Basic flow patterns

A hydraulic jump is a sudden transition that is characterized by the development of large-scale turbulence, surface waves and spray, energy dissipation, and air entrainment. At the jump toe, air bubbles, and air packets were entrained into a free shear layer characterized by intensive turbulence production, predominantly in vortices with horizontal axes perpendicular to the flow direction (Figs 1 and 2). Air entrainment occurred in the form of air bubbles and air pockets entrapped at the impingement of the upstream jet flow with the roller. The air packets were broken up in very small air bubbles as they were advected in the shear region. Once the entrained bubbles were advected into regions of lesser shear, bubble collisions and coalescence led to larger air entities (bubbles, pockets) that were driven by buoyancy towards the free-surface. In the recirculating region, unsteady flow reversal and recirculation were observed. The location of the jump toe was consistently fluctuating around its mean position and some "vortex shedding" was observed in the mixing layer.

The position of the hydraulic jump toe fluctuated with time within a 0.2–0.4-m range depending on the flow conditions. Pulsation frequencies F_{toe} of the jump toe were typically about 0.5–2 Hz for the present study. Figure 3 summarizes the observations in terms of the Strouhal number $F_{toe} * d_1/V_1$ as function of the inflow Reynolds number $Re_1 = \rho_w * V_1 * d_1/\mu_w$. The data of Long *et al.* (1991) and Mossa and Tolve (1998) are also reported in Fig. 3. The jump toe pulsations were believed to be caused by the growth, advection, and pairing of large-scale vortices in the developing shear layer of the jump (Long *et al.*, 1991; Habib *et al.*, 1994).

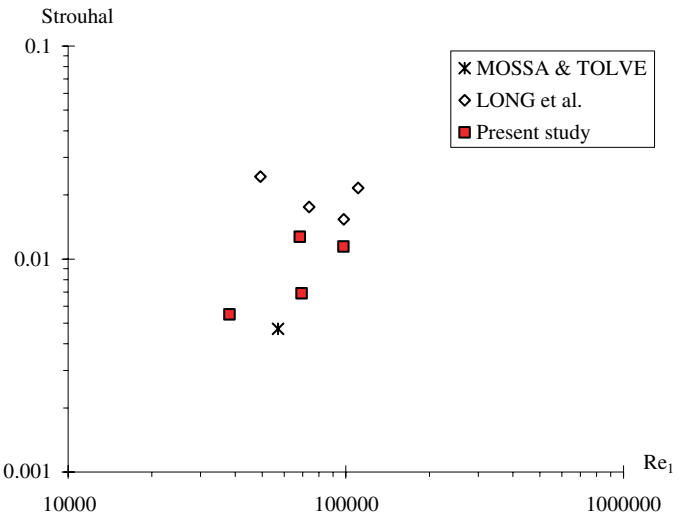

Figure 3 Hydraulic jump toe fluctuations: relationship between Strouhal and Reynolds numbers (comparison with the data of Long *et al.* (1991) and Mossa and Tolve (1998)).

4.1 Effects of Reynolds number on air–water flow patterns

When experiments with identical inflow Froude numbers were repeated in both channels, the hydraulic jump flows appeared visually more energetic in the large flume at the larger Reynolds number. This was seen using high-shutter speed photographs (Fig. 2). Figure 2A shows a photograph taken in the small flume. Little air–water projections and comparatively larger entrained air bubbles were observed. Figure 2B illustrates the same jump in the large channel with an identical inflow Froude number ($Fr_1 = 6.5$) but a larger Reynolds number. The amount of air–water projections above the jump roller was larger at the highest Reynolds number. This was associated with significant spray, splashing and waves that sometimes overtopped the channel walls. During the experiments, some spray droplets were seen at heights of more than 0.5–1 m above the invert, in the large channel. In contrast, little spray was observed in the small channel.

5 Distributions of void fraction and bubble count rate

A hydraulic jump with partially-developed inflow is characterized by a turbulent shear layer with an advective diffusion region in which the air concentration distributions exhibit a peak in the turbulent shear region (Resch and Leutheusser, 1972; Chanson, 1995; Chanson and Brattberg, 2000; Murzyn *et al.*, 2005). This feature is sketched in Figure 1. The bubble diffusion region is very similar to that observed in two-dimensional plunging jet flows (Cummings and Chanson, 1997a, b; Brattberg and Chanson, 1998). A similar advective diffusion layer was observed in the present study and it is documented experimentally in Figs 4 and 5. Figure 4A presents some longitudinal variation in void fraction distributions for one experiment. In the air diffusion layer, the peak void fraction C_{max} decreased with increasing distance $(x - x_1)$ from jump toe, while the diffusion layer broadened (Fig. 4A). The interactions between developing shear layer and air diffusion layer are complicated, and they are believed to be responsible for the existence of a peak F_{max} in bubble count rate seen in Fig. 4B. Experimental observations showed that the location where $F = F_{max}$ did not coincide with the locus of maximum void fraction.

In the air diffusion layer, the analytical solution of the advective diffusion equation for air bubbles yields the void fraction profile (Chanson, 1997; Cummings and Chanson, 1997a):

$$C = \frac{\frac{Q_{air}}{Q_w}}{\sqrt{4 * \pi * D^{\#} * \frac{x-x_1}{d_1}}} * \left(\exp\left(-\frac{1}{4 * D^{\#}} * \frac{\left(\frac{y}{d_1} - 1\right)^2}{\frac{x-x_1}{d_1}} \right) + \exp\left(-\frac{1}{4 * D^{\#}} * \frac{\left(\frac{y}{d_1} + 1\right)^2}{\frac{x-x_1}{d_1}} \right) \right) \quad (3)$$

where Q_{air} is the volume flow rate of entrained air, Q_w is the water discharge, $D^{\#}$ is a dimensionless diffusivity: $D^{\#} = D_t/(V_1 * d_1)$, D_t is the turbulent diffusivity which averages the effects of turbulent diffusion and of longitudinal velocity gradient. Equation (3) is valid for both two-dimensional supported plunging jet and hydraulic jump flows. In practice, experimental data showed that the void fraction profiles were best predicted by an approximate expression:

$$C = C_{max} * \exp\left(-\frac{1}{4D^{\#}} * \frac{\left(\frac{y}{d_1} - \frac{Y_{C_{max}}}{d_1}\right)^2}{\frac{x-x_1}{d_1}} \right) \quad \text{air diffusion later} \quad (4)$$

where C_{max} is the maximum air content in the turbulent shear layer region measured at $y = Y_{C_{max}}$ above the bottom (Fig. 1). Equation (4) is compared with experimental data in Figs. 4 and 5. Values of C_{max} and $D^{\#}$ for the best data fit are summarised in Appendix A. Overall, the order of magnitude was consistent with the earlier studies of Chanson (1995) and Chanson and Brattberg (2000).

In the present study Eq. (4) was observed only for $Re_1 > 2.5E + 4$. For lower inflow Reynolds numbers, the rate of air entrainment was weak and rapid air detrainment destroyed any organised advective diffusion layer (Fig. 5A).

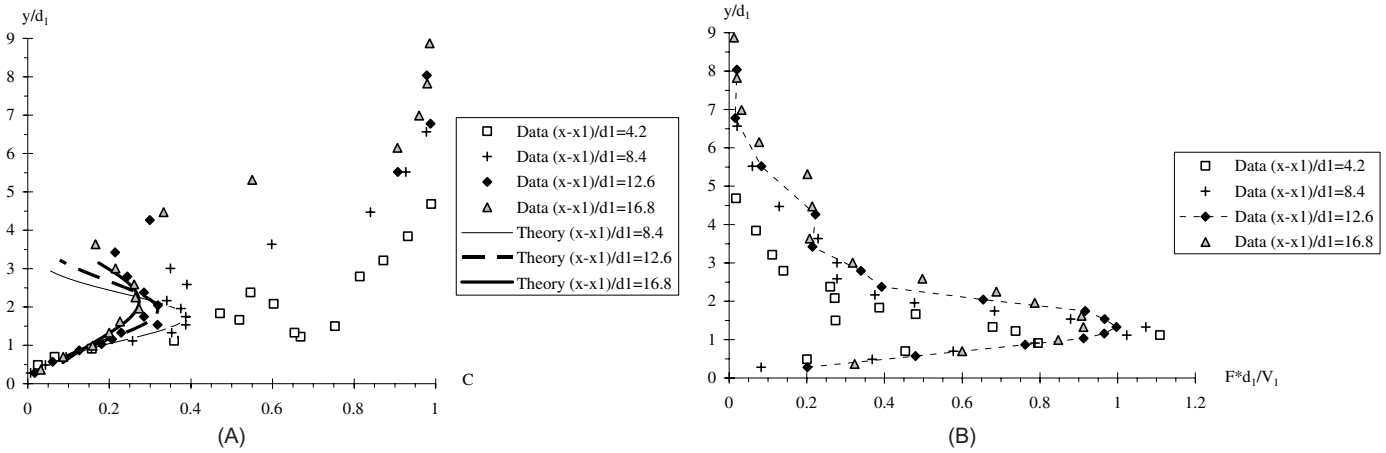

Figure 4 Dimensionless distributions of void fraction and bubble count rate $-Fr_1 = 8.6$, $Re_1 = 9.8E + 4$, $d_1 = 0.024$ m, $x_1 = 1.0$ m, $W = 0.50$ m, $x - x_1 = 0.1, 0.2, 0.4$ m. (A) Void fraction distributions (comparison with Eq. (4)). (B) Bubble count rate distributions.

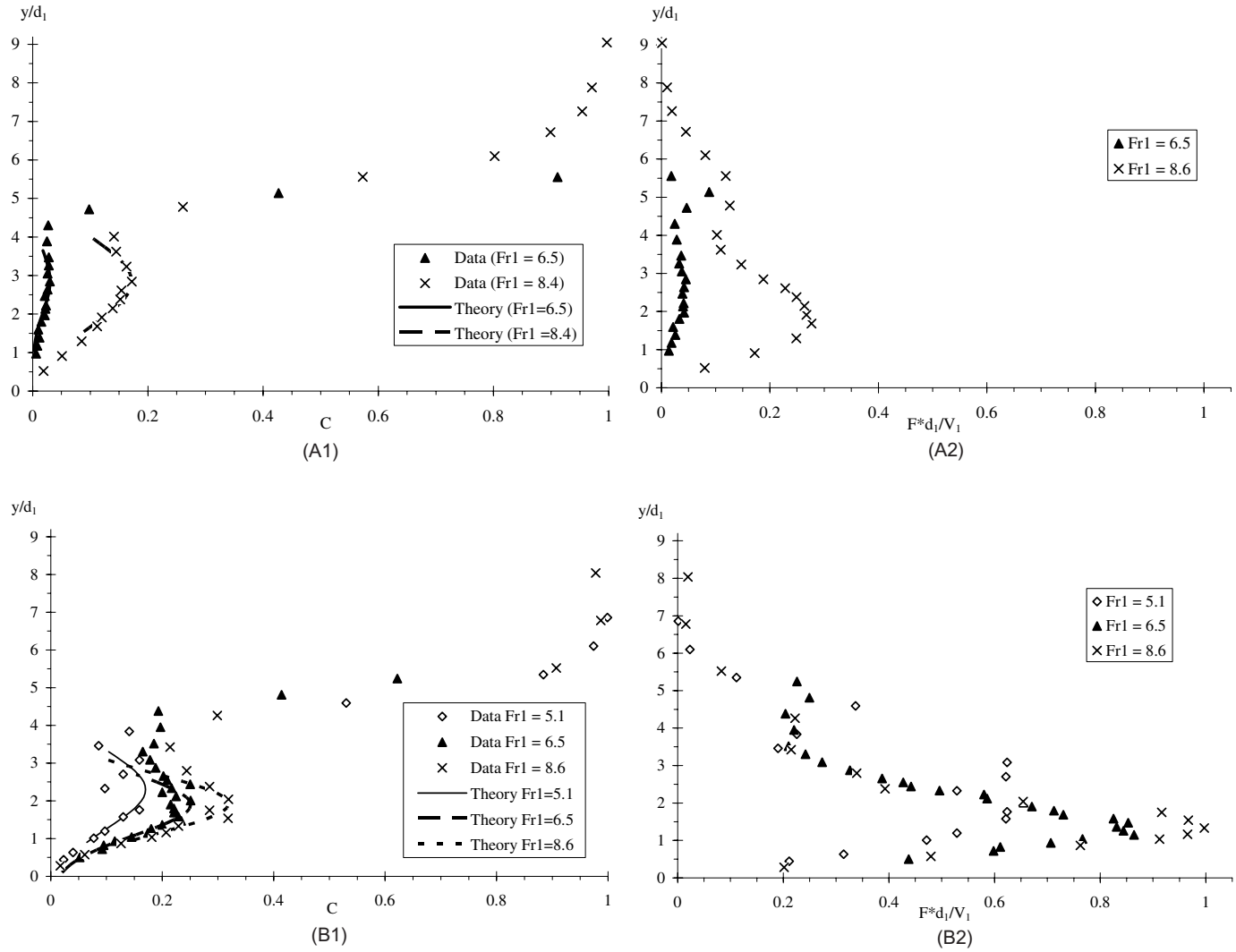

Figure 5 Effects of Reynolds number on dimensionless distributions of void fraction and bubble count rate for three inflow Froude numbers $Fr_1 = V_1/\sqrt{g * d_1}$. (A) Small flume data, $W = 0.25$ m, $x - x_1 = 0.15$ m. (A1) Void fraction distributions (comparison with Eq. (4)). (A2) Bubble count rate distributions. (B) Large flume data, $W = 0.5$ m, $x - x_1 = 0.3$ m. (B1) Void fraction distributions (comparison with Eq. (4)). (B2) Bubble count rate distributions.

5.1 Effects of Reynolds number

Similar experiments were repeated with identical inflow Froude numbers Fr_1 and relative channel width W/d_1, but different inflow Reynolds numbers Re_1. The results showed systematically that the void fraction distributions had a similar shape in the advective diffusion layer, but for $Re_1 = 2.5$E+4. In the small channel and for the lowest Froude number ($Fr_1 = 5.1$, $Re_1 = 2.5$E+4), the advective diffusion layer was not observed because the flow was not energetic enough and the bubble de-aeration process was dominant.

The longitudinal variations in void fraction distributions showed some de-aeration associated with an upward shift of the advective diffusion layer (Fig. 4A). The de-aeration rate was greater for a given inflow Froude number in the small flume as illustrated by comparing Fig. 5A and 5B which present results for identical Froude numbers but different Reynolds numbers. Further lesser dimensionless bubble count rates were recorded in the small channel at the smaller Reynolds numbers, particularly in the air–water mixing layer. For $Fr_1 = 6.5$ and $Re_1 = 2.7$E + 4, the dimensionless bubble count rate $F * d_1/V_1$ was nearly 10 times smaller then that measured in the large flume with $Fr_1 = 6.5$ and $Re_1 = 7.1$E+4 (Fig. 5A and 5B). For $Fr_1 = 8.5$, the dimensionless bubble count rates in the small channel were about 2 times smaller than those recorded at larger Reynolds number in the large flume.

Figure 5 illustrates the effects of the Reynolds number on the dimensionless distributions of void fractions and bubble count rates at one cross-section (i.e. $(x-x_1)/d_1 = 12$)) for three different inflow Froude numbers. Figure 5A presents the experimental data in the small channel and Fig. 5B shows the data in the large flume. In the advective diffusion layer, void fraction data are compared with Eq. (4).

In summary, present experiments demonstrated consistently some scale effects in terms of void fraction and bubble count rate distributions in the small channel with $Re_1 < 4$E+4 for identical Froude numbers Fr_1 ($5 \leq Fr_1 \leq 8.5$) and relative channel width W/d_1. This is illustrated in Fig. 5 presenting comparative void fraction and bubble count rate distributions in the developing flow region of hydraulic jumps with partiallydeveloped inflow.

6 Discussion: characteristics of the advective diffusion layer

Measured locations of maximum void fraction C_{max} and maximum bubble count rate F_{max}, and associated air–water flow properties, are summarised in Fig. 6. The tabular data are reported in Appendix A. In Fig. 6, experimental flow conditions are documented in the legend.

The maximum air content in the shear layer region decreased with increasing distance from the jump toe. The data followed closely some exponential decay functions as shown by Chanson and Brattberg (2000) and Murzyn *et al.* (2005). Similarly, the maximum bubble frequency was observed to decay exponentially with the distance from the impingement point. Experimental results in terms of maximum void fraction and maximum bubble count rate are shown in Figs. 6A and 6B. In Fig. 6B, present data are compared with the experimental results of Chanson and Brattberg (2000) obtained with a finer probe sensor (Ø = 0.025 mm) and the empirical correlation that they derived:

$$\frac{F_{max} * d_1}{V_1} = 0.11687 * Fr_1 * \exp\left(-0.0415 * \frac{x - x_1}{d_1}\right) \quad \text{for } \frac{x - x_1}{d_1} < 30 \tag{5}$$

Despite some general agreement with earlier data sets and empirical correlations, Fig. 6A and 6B illustrate some effect of the Reynolds number on air–water flow properties. In both Figs. 6A and 6B, the data in the upper part of the graphs correspond to the largest Reynolds numbers (white symbols), while the fastest decay in maximum void fraction and count rate occurred for the experiments with the lowest Reynolds numbers (dark symbols). It is worth commenting that Eq. (5) does not fit the present data and that it does not take into account the effects of the Reynolds number.

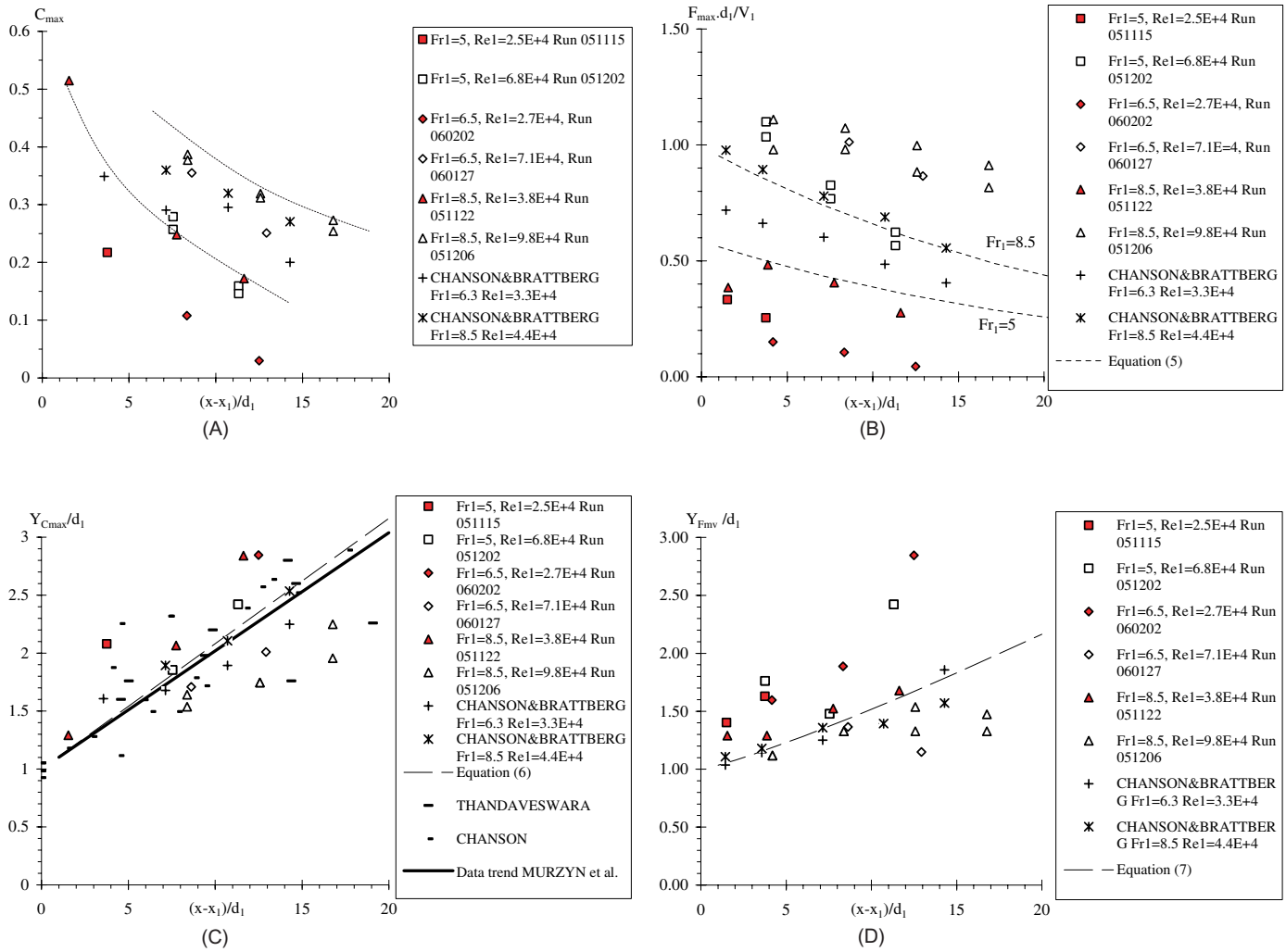

Figure 6 Longitudinal variations of maximum void fractions and bubble count rates in the advective diffusion layer of hydraulic jump with partially-developed inflow. (A) Maximum void fraction C_{max}: experimental data (present study, Chanson and Brattberg, 2000) Trendlines are shown in dotted lines. (B) Maximum dimensionless bubble count rate $F_{max} * d_1/V$: comparison between experimental data (present study, Chanson and Brattberg, 2000) and Eq. (5) for $Fr_1 = 5$ and 8.5. (C) Location of the maximum air content $Y_{C_{max}}/d_1$ in hydraulic jumps with partially developed inflow conditions: comparison between data (present study, Murzyn *et al.*, 2005; Chanson and Brattberg, 2000; Chanson, 1995; Thandasvewara, 1974) and Eq. (6). (D) Location of the maximum bubble count rate $Y_{F_{max}}/d_1$ in hydraulic jumps with partially developed inflow conditions: comparison between data (present study, Chanson and Brattberg, 2000) and Eq. (7).

The experimental observations showed systematically that the locus of maximum void fraction $Y_{C_{max}}$ was always higher than the location of maximum bubble count rate $Y_{F_{max}}$. This is shown in Figs. 6C and 6D which present the experimental data in terms of $Y_{C_{max}}/d_1$ and $Y_{F_{max}}/d_1$, respectively. The non-coincidence of the locations of maximum void fraction and bubble count rate was previously observed in hydraulic jumps (Chanson and Brattberg, 2000), in vertical supported plunging jets (Brattberg and Chanson, 1998) and in vertical circular plunging jets (Chanson *et al.*, 2004). These studies suggested that the finding was related to a double diffusion process whereas vorticity and air bubbles diffuse at a different rate and in a different manner downstream of the impingement point. There would be some dissymmetry in turbulent shear stress across the bubbly flow region which would influence the characteristic bubble size and hence the number of bubbles for a given void fraction in the advective diffusion region.

Present data are compared with earlier experimental data and the empirical correlations of Chanson and Brattberg (2000):

$$\frac{Y_{C_{max}}}{d_1} = 1 + 0.10815 * \frac{x - x_1}{d_1} \quad \frac{x - x_1}{d_1} < 30 \quad (6)$$

$$\frac{Y_{F_{max}}}{d_1} = 1 + 0.03457 * \left(\frac{x - x_1}{d_1}\right)^{1.1738} \quad \frac{x - x_1}{d_1} < 30 \quad (7)$$

Note that, in both Figs. 6C and 6D, the upper part of the graph corresponds to the lowest inflow Reynolds number experiments (dark symbols).

7 Summary and conclusion

New measurements were performed in the air entrainment region of hydraulic jumps with partiallydeveloped flow conditions (Table 1). The experiments were performed in two channels in which similar experiments with identical inflow Froude numbers and relative channel widths were conducted with a true geometric scaling ratio of $L_r = 2$ (i.e. 2:1 scale). The experimental investigations were conducted for $5 \leq Fr_1 \leq 8.5$, $2.5\text{E}+4 = Re_1 = 9.8\text{E}+4$ and $W/d_1 \approx 20$. The study is believed to be the first systematic investigation of scale effects affecting air entrainment in hydraulic jumps with an accurate air–water metrology.

Void fraction distributions showed the presence of an advection/diffusion shear layer in which the air concentration distributions followed an analytical solution of the diffusion equation for air bubbles. A similar pattern was previously observed in hydraulic jumps. However present results demonstrated that the advective diffusion layer was observed only for $Re_1 > 2.5\text{E}+4$. For smaller inflow Reynolds numbers, the air entrainment rate was relatively weak and air detrainment tended to dominate the air–water flow pattern. The results showed some scale effects in the small hydraulic jumps in terms of void fraction and bubble count rate. Void fraction distributions implied comparatively greater detrainment at low Reynolds numbers yielding to lesser overall aeration of the jump roller. Dimensionless bubble count rates were significantly lower in the smaller channel, especially in the mixing layer. The finding has direct implications on the scaling of bubble counts and interfacial areas that are proportional to the bubble count rates. Present results imply that small size model results would underestimate both bubble count rates and air–water interfacial areas.

This study complements earlier works. It shows that the hydraulic jump is a fascinating two-phase flow that is still poorly understood. It is worth noting that the present study did not account for the characteristics of the instrumentation in the physical scaling. The size of the probe sensor, scanning rate and scan duration were identical in all experiments.

Acknowledgments

The authors acknowledge the assistance of Graham Illidge and Clive Booth. The first writer thanks Prof. M. Mossa (Politecnico di Bari) and Dr F. Murzyn (Estaca) for their pertinent comments. The second writer acknowledges that the research was partly supported by the Exchange Program for Professors and Researchers of the University of Napoli "Federico II" for the year 2006.

Appendix: Air diffusion layer characteristics in hydraulic jump with partially-developed

Run	Fr_1	Re_1	$\frac{w}{d_1}$	$\frac{x_1}{d_1}$	$\frac{x - x_1}{d_1}$	$\frac{F_{max} * d_1}{V_1}$	$\frac{Y_{F_{max}}}{d_1}$	C_{max}	$\frac{Y_{C_{max}}}{d_1}$	$\frac{D_t}{d_1 * V_1}$
(1)	(2)	(3)	(4)	(5)	(6)	(7)	(8)	(9)	(10)	(11)
Small flume										
051115	5.1	2.5E+4	18.8	38	1.5	0.33	1.4	N/A	N/A	N/A
					3.8	0.25	9.8	*0.22*	*2.1*	N/A
					7.5	—	—	*0.11*	*2.4*	N/A
060202	6.5			42	8.3	0.11	1.89	0.108	—	*0.04*
					12.5	0.05	2.85	0.03	2.85	0.025
051122	8.4	3.8E+4	19.4	39	1.6	0.38	1.3	*0.515*	*1.3*	*0.004*
					3.9	0.48	1.3	N/A	N/A	N/A
					7.8	0.41	1.5	0.248	2.1	0.035
					11.6	0.28	1.7	0.172	2.8	0.055

(*continued*)

Run	Fr_1	Re_1	$\frac{w}{d_1}$	$\frac{x_1}{d_1}$	$\frac{x-x_1}{d_1}$	$\frac{F_{max} * d_1}{V_1}$	$\frac{Y_{F_{max}}}{d_1}$	C_{max}	$\frac{Y_{C_{max}}}{d_1}$	$\frac{D_t}{d_1 * V_1}$
(1)	(2)	(3)	(4)	(5)	(6)	(7)	(8)	(9)	(10)	(11)
Large flume										
051202	5.1	6.8E+4	18.9	38	3.8	1.10	1.8	N/A	N/A	N/A
					7.5	0.83	1.5	*0.279*	1.9	0.02
					11.3	0.62	2.4	*0.159*	*2.4*	0.045
060127	6.5	7.1E+4	21.6	43	8.6	1.01	1.36	0.355	1.71	0.024
					12.9	0.87	1.15	0.251	2.0	0.025
051206	8.6	9.8E+4	21.0	42	4.2	1.11	1.12	N/A	N/A	N/A
					8.4	1.07	1.33	0.387	1.6	0.022
					12.6	1.00	1.3	0.319	1.7	0.024
					16.8	0.91	1.3	0.273	2.0	0.033

Notes: $D^{\#} = D_t/(V_1 * d_1)$: dimensionless diffusivity satisfying Eq. (4); N/A: not applicable; *Italic data*: suspicious, possibly incorrect data; (—): data not available.

Notation

C = Void fraction defined as the volume of air per unit volume of air and water; it is also called air concentration or local air content
C_{max} = Maximum void fraction in the air bubble diffusion layer
D_t = Turbulent diffusivity (m^2/s) of air bubbles in air–water flow
$D^{\#}$ = Dimensionless turbulent diffusivity: $D^{\#} = D_t/(V_1 * d)1)$
d = Flow depth (m) measured perpendicular to the flow direction
d_1 = Flow depth (m) measured immediately upstream of the hydraulic jump
F = Air bubble count rate (Hz) or bubble frequency defined as the number of detected air bubbles per unit time
F_{max} = Maximum bubble count rate (Hz) in the air bubble diffusion layer
Fr_1 = Upstream Froude number: $Fr_1 = V_1/\sqrt{g * d_1}$
F_{scan} = Scanning frequency (Hz) or scan rate
F_{toe} = Hydraulic jump toe pulsation frequency (Hz)
g = Gravity constant: $g = 9.80\ m/s^2$ in Brisbane, Australia
L_r = Geometric scaling ratio defined as the prototype to model dimensions: e.g. $L_r = 2$ when the model is half the prototype size
M_o = Morton number defined as: $M_o = g * \mu_w^4/(\rho_w * \sigma^3)$
Q_{air} = Air discharge (m^3/s)
Q_w = Water discharge (m^3/s)
q_w = Water discharge per unit width (m^2/s)
Re_1 = Inflow Reynolds number: $Re_1 = \rho_w * \frac{V_1 * d_1}{\mu_w}$
T_{scan} = Scan duration (Hz) or sampling period
u' = Root mean square of longitudinal component of turbulent velocity (m/s)
u'^1 = Root mean square of longitudinal component of turbulent velocity (m/s) of the upstream flow
V = Velocity (m/s)
V_{max} = Maximum velocity (m/s) at outer edge of boundary layer
V_1 = Upstream flow velocity (m/s): $V_1 = q_w/d_1$
=
x = Distance along the channel bottom (m)
x_1 = Distance (m) between the channel intake and the hydraulic jump toe
$Y_{C_{max}}$ = Distance (m) normal to the jet support where $C = C_{max}$
$Y_{F_{max}}$ = Distance (m) normal to the jet support where $F = F_{max}$
y = Distance (m) measured normal to the invert (or channel bed)
z = Transverse distance (m) from the channel centreline
δ = Boundary layer thickness (m) defined in term of 99% of the maximum velocity: $\delta = y(V = 0.99 * V_{max})$
μ = Dynamic viscosity (Pa.s)
ρ = Density (kg/m^3)
σ = Surface tension between air and water (N/m)
Ø = Diameter (m)

Subscript

air = Air flow
w = Water flow
1 = Upstream flow conditions.

References

1. BRATTBERG, T. and CHANSON, H. (1998). "Air Entrapment and Air Bubble Dispersion at Two- Dimensional Plunging Water Jets". *Chem. Eng. Sci.* 53(24), 4113–4127. Errata: (1999) 54(12), 1925.
2. CHANSON, H. (1995). "Air Entrainment in Two-Dimensional Turbulent Shear Flows with Partially Developed Inflow Conditions". *Intl. J. Multiphase Flow* 21(6), 1107–1121.

3. CHANSON, H. (1997). *Air Bubble Entrainment in Free-Surface Turbulent Shear Flows*, Academic Press, London, UK, 401 pages.
4. CHANSON, H. (2004). *The Hydraulics of Open Channel Flows: An Introduction*, 2nd edn, Butterworth-Heinemann, Oxford, UK, 630 pages.
5. CHANSON, H. (2006). "Air Bubble Entrainment in Hydraulic Jumps. Similitude and Scale Effects". *Report No. CH57/05*, Department of Civil Engineering, The University of Queensland, Brisbane, Australia, 119 pages.
6. CHANSON, H. and BRATTBERG, T. (2000). "Experimental Study of the Air–Water Shear Flow in a Hydraulic Jump". *Intl. J. Multiphase Flow* 26(4), 583–607.
7. CHANSON, H., AOKI, S. and HOQUE, A. (2004). "Physical Modelling and Similitude of Air Bubble Entrainment at Vertical Circular Plunging Jets". *Chem. Eng. Sci.* 59(4), 747–754.
8. CUMMINGS, P.D. and CHANSON, H. (1997a). "Air Entrainment in the Developing Flow Region of Plunging Jets. Part 1: Theoretical Development". *J. Fluid. Engg. Trans. ASME*, 119(3), 597–602.
9. CUMMINGS, P.D. and CHANSON, H. (1997b). "Air Entrainment in the Developing Flow Region of Plunging Jets. Part 2: Experimental". *J. Fluid. Engg. Trans. ASME* 119(3), 603–608.
10. HABIB, E., MOSSA, M. and PETRILLO, A. (1994). "Scour Downstream of Hydraulic Jump". *Proc. Conf. Modelling, Testing and Monitoring for Hydro Powerplants*, International of Journal Hydropower and Dams, Budapest, Hungary, pp. 591–602.
11. HENDERSON, F.M. (1966). *Open Channel Flow.* MacMillan Company, New York, USA.
12. KALINSKE, A.A. and ROBERTSON, J.M. (1943). "Closed Conduit Flow". *Trans. ASCE* 108, 1435–1447.
13. LONG, D., RAJARATNAM, N., STEFFLER, P.M. and SMY, P.R. (1991). "Structure of Flow in Hydraulic Jumps". *J. Hydraul. Res. IAHR* 29(2), 207–218.
14. MOSSA, M. and TOLVE, U. (1998). "Flow Visualization in Bubbly Two-Phase Hydraulic Jump". *J. Fluid. Engg. ASME* 120, 160–165.
15. MURZYN, F., MOUAZE, D. and CHAPLIN, J.R. (2005). "Optical Fibre Probe Measurements of Bubbly Flow in Hydraulic Jumps" *Int. J. Multiphase Flow* 31(1), 141–154.
16. RAJARATNAM, N. (1962). "An Experimental Study of Air Entrainment Characteristics of the Hydraulic Jump". *J. Instn. Eng. India* 42(7), 247–273.
17. RESCH, F.J. and LEUTHEUSSER, H.J. (1972). "Le Ressaut Hydraulique: Mesure de Turbulence dans la Région Diphasique". ("The Hydraulic Jump: Turbulence Measurements in the Two-Phase Flow Region".) *J. Houille Blanche*, 4, 279–293 (in French).
18. THANDAVESWARA, B.S. (1974). "Self Aerated Flow Characteristics in Developing Zones and in Hydraulic Jumps". *Ph.D. Thesis*, Department of Civil Engineering, Indian Institute of Science, Bangalore, India, 399 pages.
19. WISNER, P. (1965). "Sur le Rôle du Critère de Froude dans l'Etude de l'Entraînement de l'Air par les Courants à Grande Vitesse". ("On the Role of the Froude Criterion for the Study of Air Entrainment in High Velocity Flows".) *Proceedings of the 11th IAHR Congress*, Leningrad, USSR, paper 1.15 (in French).